Published in final edited form as:
Nano Lett. 2012 June 13; 12(6): 3050–3061. doi:10.1021/nl300895y.

Pluronic F108 Coating Decreases the Lung Fibrosis Potential of Multiwall Carbon Nanotubes by Reducing Lysosomal Injury

Xiang Wang[†,‡,#], **Tian Xia**[†,‡,#], **Matthew C. Duch**[ζ], **Zhaoxia Ji**[‡], **Haiyuan Zhang**[‡], **Ruibin Li**[†], **Bingbing Sun**[†], **Sijie Lin**[‡], **Huan Meng**[†,‡], **Yu-Pei Liao**[†], **Meiying Wang**[†], **Tze-Bin Song**[&], **Yang Yang**[&], **Mark C. Hersam**[ζ], and **André E. Nel**[†,‡,*]

[†]Division of NanoMedicine, Department of Medicine, Northwestern University, Evanston, Illinois 60208, United States

[‡]California NanoSystems Institute, Northwestern University, Evanston, Illinois 60208, United States

[ζ]Departments of Materials Science and Engineering, Chemistry, and Medicine, Northwestern University, Evanston, Illinois 60208, United States

[&]Department of Materials Science and Engineering, University of California, Los Angeles, CA 90095, United States

Abstract

We compared the use of bovine serum albumin (BSA) and Pluronic F108 (PF108) as dispersants for multi-walled carbon nanotubes (MWCNTs) in terms of tube stability as well as pro-fibrogenic effects *in vitro* and *in vivo*. While BSA-dispersed tubes were a potent inducer of pulmonary fibrosis, PF108 coating protected the tubes from damaging the lysosomal membrane and initiating a sequence of cooperative cellular events that play a role in the pathogenesis of pulmonary fibrosis. Our results suggest that PF108 coating could be served as a safer design approach for MWCNTs.

Keywords

multiwalled carbon nanotubes (MWCNTs); Pluronic copolymer; biocompatible; dispersion; lung fibrosis

The assessment of single-wall (SW) and multi-wall (MW) carbon nanotube (CNT) toxicity is of considerable importance due to their widespread industrial use and the possibility that this could lead to human exposure in occupational and consumer settings.[1–4] Although no human disease can be attributed to CNTs at present, experimental data have demonstrated the propensity of these materials to generate frustrated phagocytosis, granulomatous inflammation, fibrosis, cytotoxicity, oxidative stress and genotoxicity.[5–17] Due to the diversity and complex physicochemical nature of CNTs it has been difficult to get a handle

[*]Corresponding Author: André E. Nel, M.D./Ph.D., Department of Medicine, Division of NanoMedicine, UCLA School of Medicine, 52-175 CHS, 10833 Le Conte Ave, Los Angeles, CA 90095-1680. Tel: (310) 825-6620, Fax: (310) 206-8107, anel@mednet.ucla.edu.
[#]Contributed equally to this work

on the exact properties that render CNTs hazardous and how to perform safety evaluation that predicts which material properties contribute to disease pathogenesis.[2, 5, 7] While it is known that the purity, length, wall number, state of aggregation, and surface chemistry of the tubes play a role in determining hazard potential, there has not been a systematic dissection of the proportional contribution of each property to the tubes' toxicological potential.[5, 7, 18, 19]

We have recently made two important advances that have helped to clarify the role of CNT aggregation status and the role of the dispersion in toxicological assessment. The first was the development of a quantitative method to assess MWCNT dispersal by bovine serum albumin (BSA) plus dipalmitoyl phosphatidylcholine (DPPC), and being able to directly relate the dispersal state of raw, purified and carboxylated tubes to their fibrogenic potential in the intact lung[20]. The second contribution was the development of a predictive toxicological paradigm that allowed us to dissect the impact of the aggregated and dispersed tubes on epithelial cells and macrophages and to relate the synergistic cellular responses to the generation of identical biomarkers that are involved in fibrogenesis in the murine lung.[21] More specifically, we demonstrated that better dispersed MWCNTs are more prone to induce the production of interleukin-1β (IL-1β), transforming growth factor-β1 (TGF-β1) and platelet-derived growth factor (PDGF-AA) *in vitro* and *in vivo* as a result of the change in cellular bioavailability as well as their ability to trigger IL-1β production through the NALP3 inflammasome.[21–32] These observations have led us to hypothesize that the state of CNT dispersal is a key factor that determines triggering of synergistic, pro-fibrogenic responses in macrophages and epithelial cells in the pathogenesis of pulmonary fibrosis.[10, 21, 23, 24]

In contrast to the above observations, Dr. Hersam's group and their collaborators demonstrated that dispersal of HiPco-synthesized SWCNT by Pluronic F108 (PF108) promotes widespread dissemination of the tubes in the rodent lung.[25] However, in stark contrast to our results with BSA-dispersed tubes, PF108 dispersal was not associated with pulmonary fibrosis and the tubes were totally cleared from the lung. Although this difference could be due to the wall number, we regarded this as unlikely and postulated that the differences reflect the effect of the dispersant on the toxicological properties of the coat tube surfaces, independent of their state of dispersal.[25] We used as-purchased (AP), purified (PD) and carboxylated (COOH) MWCNTs to perform a comparative study of BSA versus PF108 dispersal on their pro-fibrogenic effects *in vitro* and *in vivo*. We hypothesized that any possible differences could be explained by these dispersants exerting different effects on tube bioavailability or damage to the lysosome, which could lead to the activation of the NALP3 inflammasome and IL-1β production.[26, 27] Here, we demonstrate for the first time that MWCNT dispersal by PF108 leads to differences in bioavailability, cathepsin B release from lysosomes and IL-1β production in THP-1 cells as compared to BSA-dispersed tubes. Moreover, these differences were directly comparable to differences in IL-1β and TGF-β1 production and the development of pulmonary fibrosis in the lungs of CB57Bl/6 mice receiving oropharyngeal tube instillation. These results demonstrate that non-covalent modification of the MWCNT surface can be used to control the state of dispersion as well as the bioreactivity that lead to pro-fibrogenic effects. These results have important

implications for understanding CNT hazard as well as their safer design for use as nano therapeutics and imaging agents.[3]

Results and Discussion

Characterization of and dispersal of MWCNTs with PF108

Cheap Tubes Inc. supplied the raw or "as-prepared" (AP) MWCNTs, which served as the precursor for preparing purified (PD) and carboxylated (COOH) derivatives as described in our previous studies[20, 21]. AP-MWCN Ts contained ~5.25 wt % metal impurities from catalysts, including Ni (4.49 wt %) and Fe (0.76 wt %). PD-MWCNTs were prepared by purification with dilute acids, chelating agents in mild conditions.[21, 28] After purification, the metal impurity content decreased from 5.25 wt % to 1.88 wt %. Further acid treatment of the purified tubes resulted in tubes with a carboxyl content of 5.27 % of the carbon backbone (on a per weight basis). The primary bundle length of these tubes was 5–10 μm. The major physicochemical characteristics of these MWCNTs are shown in Table 1. Additional details of the MWCNT characteristics are listed in our previous publications.[21]

Pluronic® is a non-ionic triblock copolymers composed by two hydrophilic poly (ethylene oxide) (PEO) chains and an interspersed hydrophobic poly (propylene oxide) (PPO) domain.[29, 30] Previous studies have demonstrated that different polymer lengths, particularly PF127 and PF108, can achieve excellent CNT dispersal due to their amphiphilic and steric hindrance effects.[25, 29] Because this dispersal depends on the tube dimensions and the lengths of the polymeric chains, theoretical calculations and experimental data have confirmed that copolymers with longer hydrophilic segments are better dispersants than polymers with shorter hydrophilic chains.[31–34] For this reason, we chose Pluronic F108, which exhibits longer PEO blocks than F127 to perform the tube dispersals for this study.[29] In order to obtain the best possible understanding of the functional effect of PF108 dispersion, we used two dispersal methods, one in which the MWCNTs are dispersed by addition of PF108, without further purification, and the second using an additional centrifugation step to remove tube aggregates and therefore yield purified and more homogeneously dispersed tubes (Figure 1). The former preparation method, which we designated as PF108-C or crudely (C) motor dispersed tubes, involved addition of 100 μg of AP, PD or COOH-MWCNTs to 1 mL of 1% PF108 solution, followed by water bath sonication for 15 min. In contrast, the homogeneously dispersed (HD) tubes, designated PF108-HD, were prepared using similar amounts of PF108 and tubes, with the important difference that these tubes were sonicated with a probe for 1 h at 20% amplitude and then centrifuged at 32000 g for 30 min for collection of the supernatant. The latter fractionation procedure removed most of the large bundles and agglomerates as well as the carbon impurities. It also decreases the average to length of tubes to ~150 nm (Figure 1). In contrast, the PF108-C tubes were debundled but retained their original lengths in the range of 1–5 μm. As previously shown, tubes dispersed by BSA plus DPPC were considerably more tangled and agglomerated than either of the PF108-dispersed tubes (Figure 1). Taken together, the above dispersal techniques generated a graded series of tube dispersals in which the dispersal state of PF108-C was intermediary between the BSA-dispersed and the PF108-HD tubes.

The mechanism of CNT dispersion is important for understanding the biological differences between BSA- versus PF108-dispersed tubes.[20, 25, 30, 35] While the major effect of the BSA/DPPC surface coating is steric and electrosteric hindrance,[20] the principal effect of PF108 at physiological pH is to provide steric hindrance.[25, 29] This steric effect is dependent on adsorption of hydrophobic PPO midblock to the hydrophobic tube sidewalls, leading to their coating in which the hydrophilic PEO end-blocks project away from the tube surface like an array of brushes.[29] This effect is sufficient to overcome the Van der Waals forces that result in tube bundling and leads to their stable dispersion in aqueous and biological media.[29, 30] The high local shear force from sonication contributes to tube dispersal by exfoliating the bundled ends, allowing additional copolymer adsorption and stable dispersion in aqueous and tissue culture media.[29–31] This is illustrated by determining the state of dispersion of MWCNTs in RPMI 1640, one of the culture media used in this communication (Figure S1). Comparison of the suspension stability index of the tubes by following the change in the optical density of the medium over time, demonstrated that PF108-HD tubes were considerably more stable than BSA/DPPC or PF108-C dispersed tubes. The suspension stability could affect the tube bioavailability as well as their bioreactivity.

PF108, different from BSA/DPPC, decreases the pro-inflammatory potential of MWCNTs by preventing lysosomal damage in phagocytic cells

Because our ultimate goal is to compare the pro-fibrogenic effects of BSA versus PF108 dispersion in the lung, we used a recently developed *in vitro* platform to gain an understanding of the cooperation between macrophages and cellular elements of the epithelial-mesenchymal trophic (EMT) as the basis for pulmonary fibrosis.[21] The synergy between macrophage released IL-1β and TGF-β1 production by the EMT unit plays a major role in collagen production and deposition in the lung.[22, 23] In order to model the events leading IL-1β production, we used a human monomyelocytic leukemia cell line, THP-1, which differentiates into a myeloid phenotype in response to PMA/Vitamin D3 treatment.[26, 27, 36] THP-1 cells have been used successfully to look at the effect of long aspect ratio materials, such as asbestos fibers and nano wires, on the induction of IL-1β release by phagocytic cells.[11, 25, 26] This pro-inflammatory response is dependent on lysosomal damage and the assembly of the NALP3 inflammasome, which is responsible for pro-IL-1β cleavage and IL-1β release.[11,25,26] While exposure of THP-1 cells to MWCNTs dispersed by BSA/DPPC induced robust IL-1β release into the THP-1 culture medium, PF108-HD tubes failed to induce a significant response, with PF108-C dispersal leading to intermediary levels of cytokine production (Figure 2A). The overall abundance of IL-1β production was higher for AP > PD >COOH-MWCNTs, which reflect differences in their purity, hydrophobicity, and surface charge, or, of which have been demonstrated previously to determine bioreactivity.[20] Please notice that none of the MWCNT formulations or different dispersion methods had any effect on THP-1 viability as determined by conducting MTS (metabolic activity) or LDH release assays (Figure S2A and S2B).

In order to demonstrate the involvement of the NALP3 inflammasome, we used NALP3-deficient ($NALP3^{-/-}$) as well as ASC-deficient ($ASC^{-/-}$)HP-1 cells to demonstrate that gene knockout leads to abrogation of the IL-1β response to MWCNTs (Figure 2B). The initiation of this response by long aspect ratio nanomaterials is dependent on lysosomal damage,

which leads to cathepsin B release and providing a robust signal for assembly of the NALP3 subunits in phagocytic cells.[27, 36] The role of cathepsin B was confirmed by using a cathepsin B inhibitor, CA-074 methyl ester, to show interference in IL-1β production (Figure 2C). Similar results were found when using the peptide, z-VYAD-fmk, to inhibit the activity of caspase 1, the NALP3 subunit that is directly involved in pro-IL-1β cleavage (Figure 2D).

In order to more directly study the effect of the various dispersal methods on lysosomal injury, we also employed a fluorescent cathepsin B substrate, Magic Red™, to visualize the localization of this enzyme in THP-1 cells by confocal microscopy. Use of monosodium urate (MSU) crystals as a positive control demonstrated that the red punctate fluorescence of Magic Red™, confined to intact lysosomes in non-treated cells, changed to a diffuse red fluorescence pattern in the cytoplasm upon from the damaged lysosomes (Figure 3A). Although AP tubes dispersed by BSA/DPPC demonstrated similar ability to induce lysosomal damage, PF108-HD tubes had no effect, while the PF108-C tubes induced lysosomal rupture (Figure 3B). Almost identical data were obtained when analyzing PD-MWCNTs (Figure S3A). While COOH-MWCNTs did not induce cathepsin B release at 4 h (Figure S3B), there was lesser amount of lysosomal damage at later time points (data not shown). Thus, the confocal data is in accordance with the IL-1β data.

In order to reconcile these studies with the cellular bioavailability of the tubes, we checked whether there is a difference in the cellular uptake for the different dispersion methods. While it was easy to identify BSA- and PF108-C dispersed tubes inside THP-1 cells using confocal Raman analysis, we could not detect PF108-HD tubes in these cells (Figure 4A and Figure S4A, S4B). This was confirmed by light optical microscopy of the cells (Figure 4A) as well as transmission electron microscopy (TEM), which showed little cellular uptake of PF108-HD tubes whereas BSA- and PF108-C dispersed tubes could be observed in membrane-lined cellular vesicles in the cell (Figure 4B and Figure S5A, S5B). These results indicate that different methods of dispersion and different dispersants affect cellular uptake by a mechanism that still needs to be determined. While the dispersion stability could play a role in determining contact of non-stabilized tubes with the cells, another possibility is that steric hindrance of PF108-HD tubes prevents cellular contact and uptake. Instead, BSA/DPPC coating could provide tube dispersal through electrosteric hindrance until these tubes make contact with the cell membrane, whereupon BSA could act as a ligand that stimulates cellular uptake.[37, 38] It is therefore interesting that the endocytosis inhibitor, cytochalasin D could significantly interfere in IL-1β production in BSA-dispersed tubes (not shown).

In addition to possible effects on cellular uptake, consideration also needs to be given to the role of the different dispersants inside the cell, as demonstrated by the confocal data as well as the finding that even though PF108-C dispersed tubes are taken up in THP-1 cells, they induce less IL-1β production than BSA-coated tubes (Figure 2A). While this could reflect a quantitative difference in the abundance of cellular uptake (which is not easy to quantify), another possibility is that the PF108 coating may interfere in the bioreactivity of the tubes inside the lysosome.[11] Although it is difficult to directly study tube interactions with the lysosomal membrane for a molecular explanation, we were able to look at the behavior of the tubes surface under experimental conditions that utilize a phagolysosomal simulant fluid

(PSF), which exhibits a pH of 4.5.[39, 40] First, we used a semi-quantitative method to detect available surface for absorption of fluorescein isothiocyanate (FITC), which binds to the MWCNT surface by π-π stacking and undergoes fluorescence quenching in the process.[41] This reaction reflects the excitation of ground-state electrons in FITC to the highest occupied molecular orbital, following which electron transfer to the CNT conduction band and then to the ground state leads to energy release in the form of thermal radiation.[39] Quantification of the fluorophore quenching is an indirect measure of the available tube surface for FITC binding.[42] Thus, the degree of quenching could be used to provide a comparison between different coated tubes, but should not be interpreted as accurate measurement of the total surface area (which changes in response to tube agglomeration).[20] For making comparisons, we assumed that the available surface for FITC binding to the surface AP-MWCNTs in the presence of PBS without any dispersant constitutes the maximal (100 %) available surface area. Figure 4C and D show the comparative surface area for FITC binding to AP-MWCNTs that were suspended in PBS or PSF in the absence and presence of BSA and PF108. This demonstrates that tube dispersal in BSA shows a dramatic decrease in the available surface area in PBS, but that this effect is partially reversed by PSF (Figure 4C), likely because albumin (isoelectric point of 4.7) undergoes a conformational change that leads to its attachment to the tube surface at a pH of 4.5. This would allow the Van der Waals forces to resume tube agglomeration, and suspension instability as suggested by the diagram in Figure S6A. In contrast, the relative available surface area for PF108 coated tubes in the presence of PBS is ~ 90% and drops to 60% in PSF (Figure 4D). However, the state of the tubes' suspendability in PSF likely remains high (Figure S6A), likely because the polymer attachment remains intact under acidic conditions, with the added possibility that binding of protons to the terminal PEO hydroxyl groups provide electrostatic repulsion. All considered, the data from the simulated lysosomal conditions suggest an important difference in the suspension stability of BSA-coated *vs*. PF108-coated tubes. While the former tubes may come out of solution and interact directly with the lysosomal membrane, PF108 coating may prevent this from happening and therefore serve to protect the lysosomal membrane. A proposed visual diagram to explain the data is included in Figure S6B. Similarly, recent studies have shown that SWCNTs coated with Pluronic as well as bovine fibrinogen also exhibit substantial decreases in cytotoxicity.[25, 43,44]

PF108, different from BSA/DPPC, decreases TGF-β1 production in BEAS-2B cells

The epithelial cell is an important component of the trophic cell unit undergoing epithelial-mesenchymal transition in the lung during development of fibrosis.[21, 23] The production of TGF-β1 by the epithelial cells contributes in synergistic fashion to the establishment of a matrix synthesis phenotype and collagen synthesis by the participating mesenchymal cellular elements.[22] We chose BEAS-2B cells, a human lung epithelial cell line, to determine whether the different dispersal methods impact the synthesis of this growth factor as determined by conducting an ELISA of the supernatant. Assessment of the suspension stability index indicates that PF108 provides excellent tube stabilization in BEGM compared to BSA (Figure S7). Similar to THP-1 cells, none of the tubes or dispersants was associated with cytotoxicity in BEAS-2B cells (Figure S8A and S8B). Although BSA-dispersed tubes induced TGF-β1 production, PF108-HD tubes did not induce TGF-β1 production (Figure

S9). PF108-C tubes also induced TGF-β1 production, which was less than the effect of BSA-coated tubes. COOH-MWCNTs induced little TGF-β1 production irrespective of the dispersal method. These TGF-β1 data are consistent with the cellular uptake of BSA- and PF108-C dispersed AP- and PD-MWCNTs in BEAS-2B cells, whereas the COOH-MWCNTs and PD108-HD tubes were not taken up to any noticeable degree (Figure S10). Taken together with the IL-1β data, these results show that PF108 coating reduces the pro-fibrogenic effects of MWCNTs compared to their dispersal by BSA.

Acute oropharyngeal aspiration in mice demonstrates the protective effect of PF108 coating on IL-1β production in the lung compared to BSA

We have previously demonstrated for MWCNTs that the *in vitro* pro-fibrogenic responses in THP-1 and BEAS-2B cells accurately reflect their ability to generate similar biomarker responses in the bronchoalveolar lavage fluid (BALF) of mice receiving oropharyngeal aspiration.[20] Because we have also learned from these studies that IL-1β production in the intact lung is an early macrophage activation event that precedes the cascade of PDGF-AA and TGF-β1 production,[22–24] we first assessed the effects of the three dispersion methods on oropharyngeal aspiration of AP-MWCNTs in C57Bl/6 mice at 40 h. We chose an exposure dose of 2 mg/kg based on the real-life assessment of exposure conditions in a MWCNT production laboratory as well as our own previous demonstration that this dose falls on the steep part of the dose-response curve of this particular tube formulation.[12,45] Moreover, this dose could also be reconciled with a surface area dose of 10–100 μg/mL in a tissue culture dish when expressing the *in vivo* dose as mass per unit alveolar surface area in the mouse.[21, 46, 47]

First, we determined that there is excellent suspension stability of the PF108 coated tubes in PBS (Figure S11). Forty hours after their oropharyngeal aspiration both PF108-HD and PF108-C tubes failed to increase IL-1β production in the BALF compared to the untreated control (Figure 5A). However, both Min-U-Sil (positive control) and BSA-dispersed tubes increased IL-1β production (Figure 5A). This is in agreement with the THP-1 results (Figure 2A). However, quite different from the THP-1 uptake data, there was good tube uptake in alveolar macrophages, irrespective of the dispersal method (Figure 5B). The intracellular presence of the tubes in macrophages was confirmed by confocal Raman microscopy, which demonstrated the classical Raman peaks for MWCNTs (Figure 5B). The same was also true for PD and COOH-MWCNTs (not shown). A possible explanation for the differences in the bioavailability *in vitro* and *in vivo* is that the PBS carrier is absorbed or removed after instillation, allowing the tubes to be deposited in the airways, where they are phagocytosed by macrophages. We also collected alveolar macrophages from the fluid for staining with Magic Red™, which demonstrated that there is diffused dye leakage into the cytosol of animals receiving BSA-dispersed tubes (Figure 5C). However, while the same degree of lysosomal damage was not obvious in macrophages obtained from the animals treated with PF108-C and PF108-HD tubes, the lysosomes appeared somewhat bigger than in control cells (Figure 5C). Nonetheless, this demonstrates the protective effect of PF108 coating is also carried through to the intact lung and could protect against pulmonary fibrosis.

Twenty one day post-exposure studies in the mouse lung to compare the fibrogenic potential of PF108 *vs*. BSA-coated MWCNTs

The murine experiment was repeated, except that the animals were sacrificed 21 days after the oropharyngeal inspiration of AP, PD, and COOH-MWCNTs. Examination of the fluid showed that while there was a significant increase in TGF-β1 (Figure 6A) and PDGF-AA (Figure 6B) production in response to all the BSA-dispersed tubes, no significant increase occurred when tubes were dispersed by either of the PF108 coating methods. Moreover, the PF108-coated tubes also did not increase collagen production in the lung, as determined by the Sircol collagen assay, while Min-U-Sil (positive control) or tubes dispersed by BSA could induce a significant effect (Figure 6C). These differences were confirmed by Masson's trichrome staining, which showed increased collagen deposition around airways and alveolar spaces of mice receiving BSA-dispersed AP and PD tubes (Figure 7). In contrast, no trichrome staining was seen in the lungs of animals receiving PF108-dispersed or COOH-MWCNTs. In agreement with the BAL fluid findings (Figure 5B), macrophages located in the alveoli or fibrotic lung regions could be observed to contain intracellular CNTs, irrespective of the type of dispersant (Figure S12). The presence of MWCNTs in these lung sites was confirmed by confocal Raman microscopy (not shown), confirming that the major protective effect of PF108 is likely at the subcellular level. Min-U-Sil induced growth factor production was accompanied by collagen deposition (Figure 6 and 7).

In summary, Pluronic coating not only confers excellent MWCNT dispersion, but also reduces the pro-fibrogenic effects of these tubes *in vitro* and in intact animal lungs. The mechanism of this effect appears to be prevention of lysosomal damage in macrophages as well as possibly other cell types. PF108 appears to passivate the tube surface by forming a protective “brush-like” layer that provides steric hindrance and interferes in tube aggregation as well as damaging interactions with the lysosomal membrane. In contrast, tube dispersal by BSA plus DPPC provides tube dispersal that do not protect the lysosome, likely because of the instability of this coating in the acidified, organellar environment. While we do not understand the exact molecular mechanism by which tubes induced lysosomal membrane damage, it was possible to demonstrate that BSA-coated tubes leads to cathepsin B release and IL-1β production in phagocytic cells (Figure S13). In contrast, the PF108 coating appears to be more resistant to removal from the surface under acidic conditions. These results suggest that PF108 coating could be used as a safe design approach for MWCNTs when considering their possible use for biomedical applications such as drug delivery and imaging. This communication also demonstrates that it is possible to use a predictive toxicological approach in which the assessment of *in vitro* effects can be used to project the *in vivo* hazard potential of carbon nanotubes.

MATERIALS AND METHODS

Carbon nanotubes and chemicals

The methodology for detailed characterization of MWCNTs is described in the Supporting Information. Briefly, MWCNT powder was purchased from Cheap Tubes Inc. (Brattleboro, VT, USA). The starting material is designated as as-prepared (AP) MWCNTs. The

purification and functionalization of the MWCNTs were accomplished as previously described.[21, 28] Pluronic F108 was obtained from BASF (BASF Corporation, NJ, USA).

Preparation of MWCNT suspensions with BSA/DPPC and PF108

All tubes (AP, PD and COOH-MWCNTs) were obtained as dry powders and prepared in deionized H2O at 5 mg/mL as stock solutions. For BSA/DPPC dispersal, both dispersants were added at 0.6 mg/mL and 0.01 mg/mL, respectively, before adding the 5 mg/mL stock solution. To obtain highly dispersed PF108 tubes, ~33 mg of powder was added to 12 mL of 1% w/v PF108 aqueous solution then sonicated by a Fisher Scientific Model 500 Scientific Dismembrator for 1 h at 20 % amplitude. These tubes were subsequently centrifuged at 32000 g for 30 min and the supernatant retained as the homogeneously dispersed (PF108-HD) stock solution. For the cruder stock (PF108-C), we added 20 μL of a 5 mg/mL MWCNTs stock solution into 1 mL 1% PF108 containing tissue culture media or PBS to obtain a 100 μg/mL working concentration and then sonicated in a water bath. Detailed protocols are in supporting information.

Cellular culture and co-incubation with MWCNTs

BEAS-2B and THP-1 cells were obtained from ATCC (Manassas, VA). 1×10^4 BEAS-2B cells were cultured in 0.2 mL BEGM in 96-well plates at 37 °C. THP-1 cells were cultured in RPMI 1640 supplemented with 10% fetal bovine serum. Before MWCNT exposure, THP-1 cells were pretreated with Vitamin D3 at 150 nM for 18 h and primed with 10 ng/mL lipopolysaccharide (LPS) to initiate the IL-1β precursor. 2.5×10^4 primed cells were seeded in 0.2 mL complete medium in 96-well plates. Following exposure to the tubes for 24 h, the supernatants from both cultures were collected to measure TGF-β1 or IL-1β by ELISA. This is described in the supporting information.

Pulmonary exposure effects

Eight-week-old male C57Bl/6 mice were exposed to BSA/DPPC-dispersed, PF108-HD and PF108-C tubes *via* oropharyngeal aspiration. Briefly, 2 mg/kg of each type of MWCNT was instilled at the back of the tongue in 50 μL PBS in anesthetized animals. Control animals received the same volume of PBS with BSA (0.6 mg/mL) and DPPC (0.01 mg/mL) or 1% PF108. 5 mg/kg crystalline silica (Min-U-Sil) was used as positive control. The mice were sacrificed at 40 hours and 21 days, BAL fluid and lung tissue were collected for measurement of TGF-β1, IL-1β and PDGF-AA levels and performance of Masson's trichrome staining.[48] The detailed methods appear in the supporting information.

Supplementary Material

Refer to Web version on PubMed Central for supplementary material.

Acknowledgments

We thank Dr. Somenath Mitra (New Jersey Institute of Technology, Newark, NJ) for providing MWCNTs to the NIEHS RC2 consortium. This work is supported by the US Public Health Service Grants (RO1 ES016746, and U19 ES019528). Infrastructure support was also provided by National Science Foundation and the Environmental Protection Agency under Cooperative Agreement Number, DBI 0830117. Dr. Hersam is also supported by U.S. National Science Foundation DMR-1006391. Fluorescent microscopy was performed at the CNSI Advanced Light

Microscopy/Spectroscopy Shared Facility at UCLA. Any opinions, findings, conclusions or recommendations expressed herein are those of the author(s) and do not necessarily reflect the views of the National Science Foundation or the Environmental Protection Agency. This work has not been subjected to an EPA peer and policy review. The findings and conclusions in this article are those of the authors and do not necessarily represent the views of the National Institute for Occupational Safety and Health.

REFERENCES AND NOTES

1. Baughman RH, Zakhidov AA, de Heer WA. Science. 2002; 297(5582):787–792. [PubMed: 12161643]
2. Nel A, Xia T, Madler L, Li N. Science. 2006; 311(5761):622–627. [PubMed: 16456071]
3. Liu Z, Tabakman S, Welsher K, Dai HJ. Nano Res. 2009; 2(2):85–120. [PubMed: 20174481]
4. Hersam MC. Nat Nanotechnol. 2008; 3(7):387–394. [PubMed: 18654561]
5. Muller J, Huaux F, Fonseca A, Nagy JB, Moreau N, Delos M, Raymundo-Pinero E, Beguin F, Kirsch-Volders M, Fenoglio I, Fubini B, Lison D. Chem Res Toxicol. 2008; 21(9):1698–1705. [PubMed: 18636756]
6. Lee JH, Lee SB, Bae GN, Jeon KS, Yoon JU, Ji JH, Sung JH, Lee BG, Lee JH, Yang JS, Kim HY, Kang CS, Yu IJ. Inhal Toxicol. 2010; 22(5):369–381. [PubMed: 20121582]
7. Oberdorster G, Maynard A, Donaldson K, Castranova V, Fitzpatrick J, Ausman K, Carter J, Karn B, Kreyling W, Lai D, Olin S, Monteiro-Riviere N, Warheit D, Yang H, Group IRFRSINTSW. Part Fibre Toxicol. 2005; 2:8. [PubMed: 16209704]
8. Shvedova AA, Kisin E, Murray AR, Johnson VJ, Gorelik O, Arepalli S, Hubbs AF, Mercer RR, Keohavong P, Sussman N, Jin J, Yin J, Stone S, Chen BT, Deye G, Maynard A, Castranova V, Baron PA, Kagan VE. Am J Physiol-Lung C. 2008; 295(4):L552–L565.
9. Jia G, Wang HF, Yan L, Wang X, Pei RJ, Yan T, Zhao YL, Guo XB. Environ Sci Technol. 2005; 39(5):1378–1383. [PubMed: 15787380]
10. Mercer RR, Scabilloni J, Wang L, Kisin E, Murray AR, Schwegler-Berry D, Shvedova AA, Castranova V. Am J Physiol-Lung C. 2008; 294(1):L87–L97.
11. Palomaki J, Valimaki E, Sund J, Vippola M, Clausen PA, Jensen KA, Savolainen K, Matikainen S, Alenius H. Acs Nano. 2011; 5(9):6861–6870. [PubMed: 21800904]
12. Porter DW, Hubbs AF, Mercer RR, Wu N, Wolfarth MG, Sriram K, Leonard S, Battelli L, Schwegler-Berry D, Friend S, Andrew M, Chen BT, Tsuruoka S, Endo M, Castranova V. Toxicology. 2010; 269(2–3):136–147. [PubMed: 19857541]
13. Ryman-Rasmussen JP, Cesta MF, Brody AR, Shipley-Phillips JK, Everitt JI, Tewksbury EW, Moss OR, Wong BA, Dodd DE, Andersen ME, Bonner JC. Nat Nanotechnol. 2009; 4(11):747–751. [PubMed: 19893520]
14. Nagai H, Okazaki Y, Chew SH, Misawa N, Yamashita Y, Akatsuka S, Ishihara T, Yamashita K, Yoshikawa Y, Yasui H, Jiang L, Ohara H, Takahashi T, Ichihara G, Kostarelos K, Miyata Y, Shinohara H, Toyokuni S. P Natl Acad Sci USA. 2011; 108(49):E1330–E1338.
15. Donaldson K, Murphy FA, Duffin R, Poland CA. Particle and fibre toxicology. 2010; 7
16. Lam CW, James JT, McCluskey R, Hunter RL. Toxicol Sci. 2004; 77(1):126–134. [PubMed: 14514958]
17. Warheit DB, Laurence BR, Reed KL, Roach DH, Reynolds GAM, Webb TR. Toxicol Sci. 2004; 77(1):117–125. [PubMed: 14514968]
18. Wang X, Jia G, Wang H, Nie H, Yan L, Deng XY, Wang S. J Nanosci Nanotechno. 2009; 9(5): 3025–3033.
19. Murphy FA, Poland CA, Duffin R, Al-Jamal KT, Ali-Boucetta H, Nunes A, Byrne F, Prina-Mello A, Volkov Y, Li SP, Mather SJ, Bianco A, Prato M, MacNee W, Wallace WA, Kostarelos K, Donaldson K. Am J Pathol. 2011; 178(6):2587–2600. [PubMed: 21641383]
20. Wang X, Xia T, Ntim SA, Ji ZX, George S, Meng H, Zhang H, Castranova V, Mitra S, Nel AE. Acs Nano. 2010; 4(12):7241–7252. [PubMed: 21067152]
21. Wang X, Xia T, Ntim SA, Ji Z, Lin S, Meng H, Chung C, George S, Zhang H, Wang M, Li N, Yang Y, Castranova V, Mitra S, Bonner J, Nel AE. ACS nano. 2011; 5(12):9772–9787. [PubMed: 22047207]

22. Bonner JC. Cytokine Growth F R. 2004; 15(4):255–273.
23. Bonner JC. Fibrogenesis & tissue repair. 2010; 3:15. [PubMed: 20738867]
24. Shvedova AA, Kisin ER, Mercer R, Murray AR, Johnson VJ, Potapovich AI, Tyurina YY, Gorelik O, Arepalli S, Schwegler-Berry D, Hubbs AF, Antonini J, Evans DE, Ku BK, Ramsey D, Maynard A, Kagan VE, Castranova V, Baron P. Am J Physiol-Lung C. 2005; 289(5):L698–L708.
25. Mutlu GM, Budinger GRS, Green AA, Urich D, Soberanes S, Chiarella SE, Alheid GF, McCrimmon DR, Szleifer I, Hersam MC. Nano Lett. 2010; 10(5):1664–1670. [PubMed: 20377197]
26. Dostert C, Petrilli V, Van Bruggen R, Steele C, Mossman BT, Tschopp J. Science. 2008; 320(5876):674–677. [PubMed: 18403674]
27. Tschopp J, Schroder K. Nat Rev Immunol. 2010; 10(3):210–215. [PubMed: 20168318]
28. Wang YB, Iqbal Z, Mitra S. J Am Chem Soc. 2006; 128(1):95–99. [PubMed: 16390136]
29. Granite M, Radulescu A, Pyckhout-Hintzen W, Cohen Y. Langmuir. 2011; 27(2):751–759. [PubMed: 21155544]
30. Ciofani G, Raffa V, Pensabene V, Menciassi A, Dario P. Fullerenes, Nanotubes and Carbon Nanostructures. 2009; 17:11–25.
31. Shvartzman-Cohen R, Nativ-Roth E, Baskaran E, Levi-Kalisman Y, Szleifer I, Yerushalmi-Rozen R. J Am Chem Soc. 2004; 126(45):14850–14857. [PubMed: 15535711]
32. Duch MCBGR, Liang YT, Soberanes S, Urich D, Chiarella SE, Campochiaro LA, Gonzalez A, Chandel NS, Hersam MC, Mutlu GM. Nano Lett. 2011; 11(12):5201–5207. [PubMed: 22023654]
33. Antaris AL, Seo JWT, Green AA, Hersam MC. ACS nano. 2010; 4(8):4725–4732. [PubMed: 20669897]
34. Seo JWT, Green AA, Antaris AL, Hersam MC. J Phys Chem Lett. 2011; 2(9):1004–1008.
35. Arutyunyan NR, Baklashev DV, Obraztsova ED. Eur Phys J B. 2010; 75(2):163–166.
36. Hamilton RF, Wu NQ, Porter D, Buford M, Wolfarth M, Holian A. Part Fibre Toxicol. 2009:6. [PubMed: 19284582]
37. Holt BD, Dahl KN, Islam MF. Small. 2011; 7(16):2348–2355. [PubMed: 21626688]
38. Yaron PNHBD, Short PA, Lösche M, Islam MF, Dahl KN. J Nanobiotechnology. 2011; 9(45)
39. Li RB, Wu RA, Wu MH, Zou HF, Ma H, Yang L, Le XC. Electrophoresis. 2009; 30(11):1906–1912. [PubMed: 19522016]
40. Stefaniak AB, Day GA, Hoover MD, Breysse PN, Scripsick RC. Toxicology in vitro : an international journal published in association with BIBRA. 2006; 20(1):82–95. [PubMed: 16061346]
41. Li RB, Wu R, Zhao L, Wu MH, Yang L, Zou HF. Acs Nano. 2010; 4(3):1399–1408. [PubMed: 20148593]
42. Li RB, Wu RA, Zhao LA, Hu ZY, Guo SJ, Pan XL, Zou HF. Carbon. 2011; 49(5):1797–1805.
43. Ge CC, Du JF, Zhao LN, Wang LM, Liu Y, Li DH, Yang YL, Zhou RH, Zhao YL, Chai ZF, Chen CY. P Natl Acad Sci USA. 2011; 108(41):16968–16973.
44. Holt BD, Short PA, Rape AD, Wang YL, Islam MF, Dahl KN. Acs Nano. 2010; 4(8):4872–4878. [PubMed: 20669976]
45. Han JH, Lee EJ, Lee JH, So KP, Lee YH, Bae GN, Lee SB, Ji JH, Cho MH, Yu IJ. Inhal Toxicol. 2008; 20(8):741–749. [PubMed: 18569096]
46. Stone KC, Mercer RR, Gehr P, Stockstill B, Crapo JD. Am J Resp Cell Mol. 1992; 6(2):235–243.
47. Xia T, Zhao Y, Sager T, George S, Pokhrel S, Li N, Schoenfeld D, Meng H, Lin SJ, Wang X, Wang MY, Ji ZX, Zink JI, Madler L, Castranova V, Lin S, Nel AE. ACS nano. 2011; 5(2):1223–1235. [PubMed: 21250651]
48. Li N, Wang MY, Bramble LA, Schmitz DA, Schauer JJ, Sioutas C, Harkema JR, Nel AE. Environ Health Persp. 2009; 117(7):1116–1123.

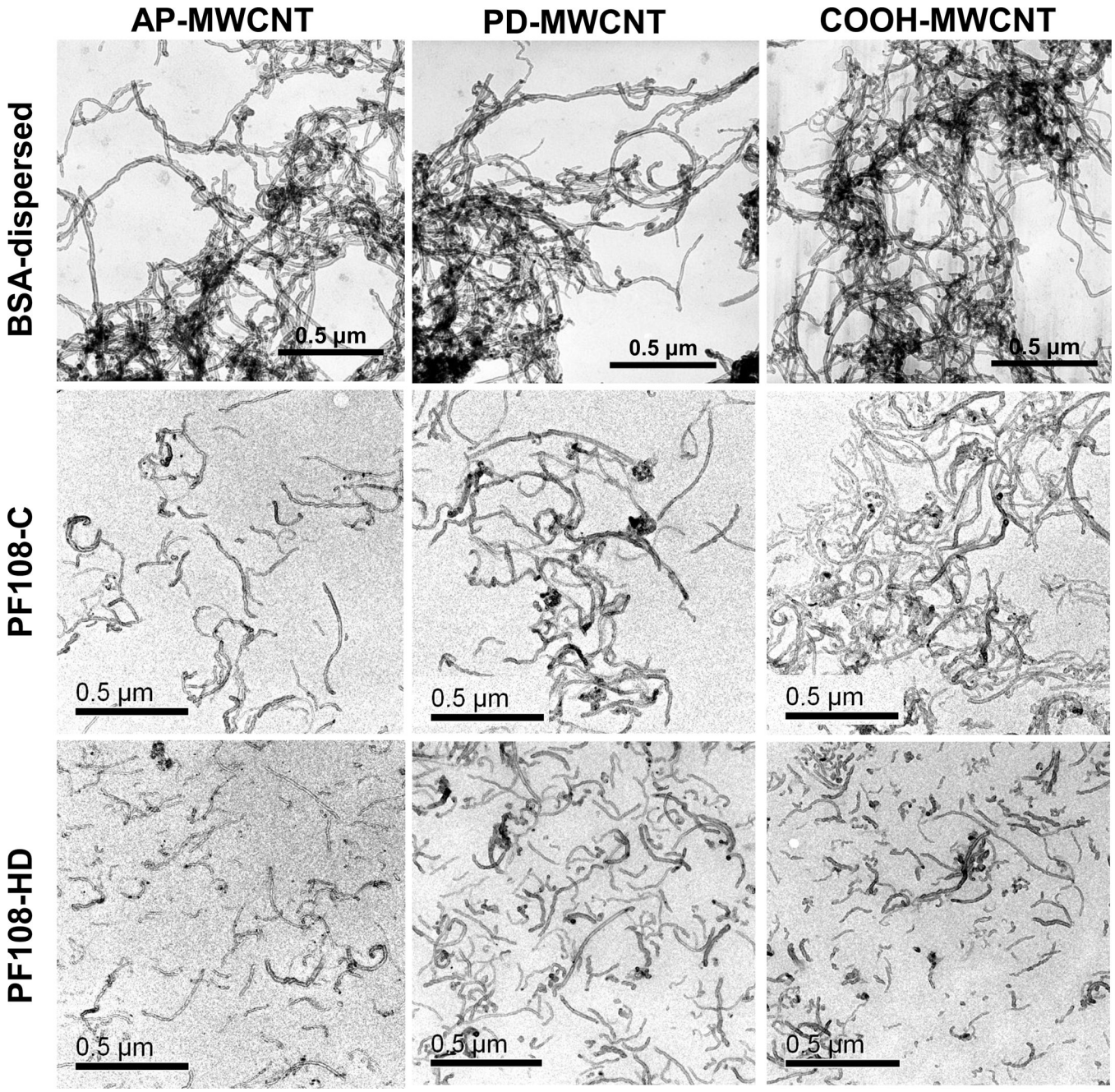

Figure 1. Representative transmission electron microscopy (TEM) images of BSA-dispersed, PF108-C and PF108-HD MWCNTs

Pictures of the AP, PD, and COOH-MWCNTs were taken with a JEOL 100 CX transmission electron microscope at 80 kV in the UCLA BRI Electron Microscopy Core. AP: as prepared; PD: purified; COOH: carboxylated; PF-C: PF108-crudely dispersed; PF-HD: PF108-homogeneously dispersed.

A

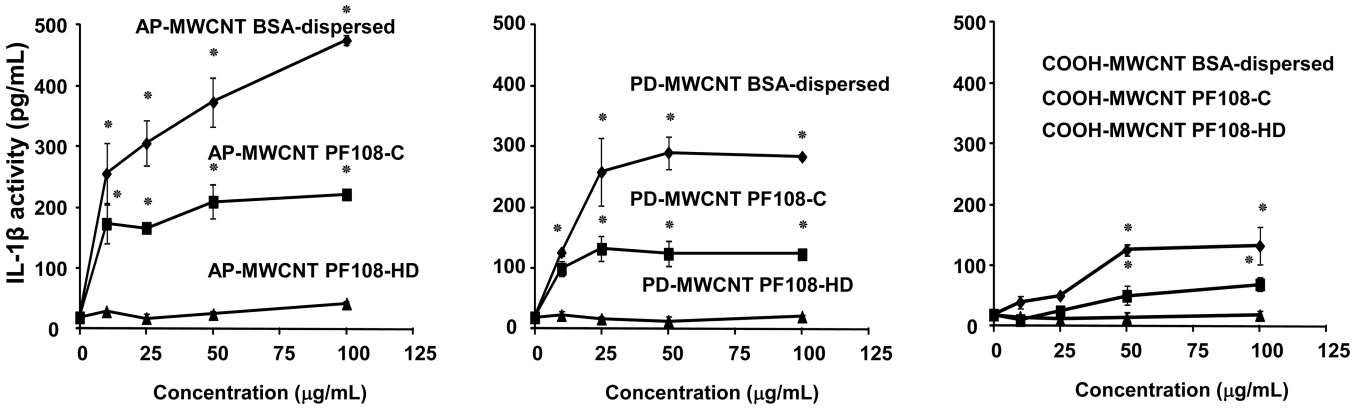

B

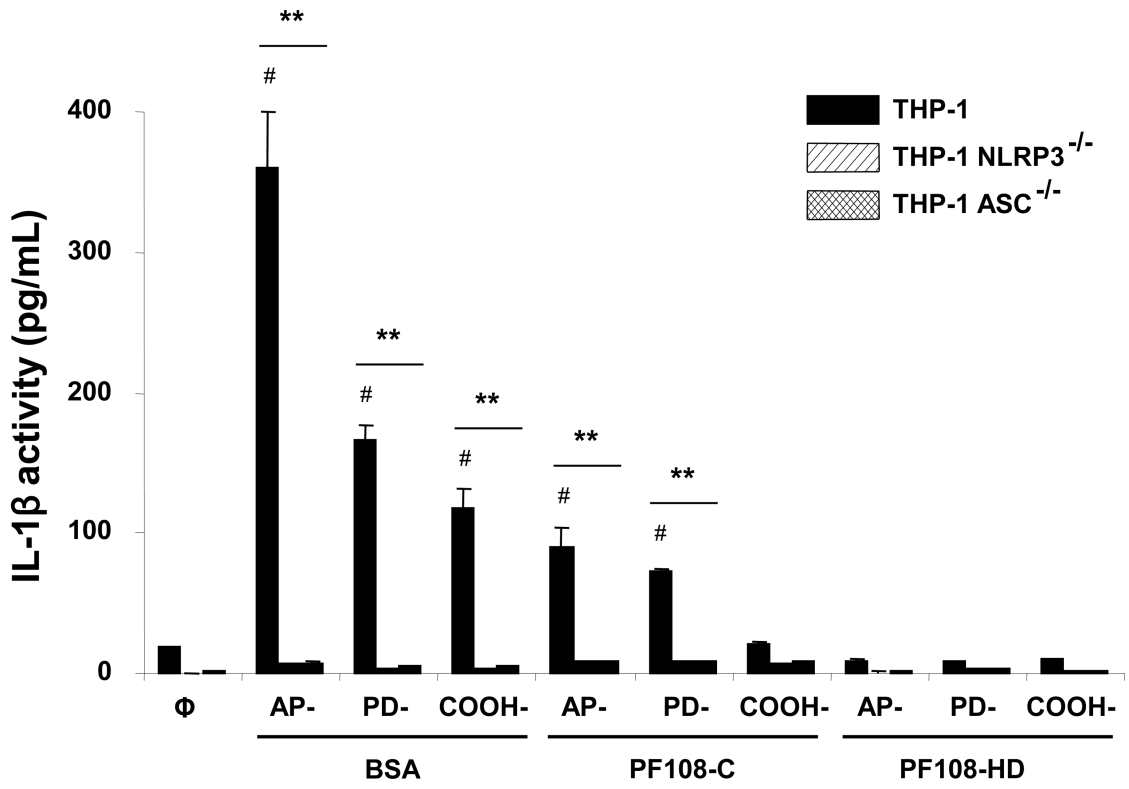

C

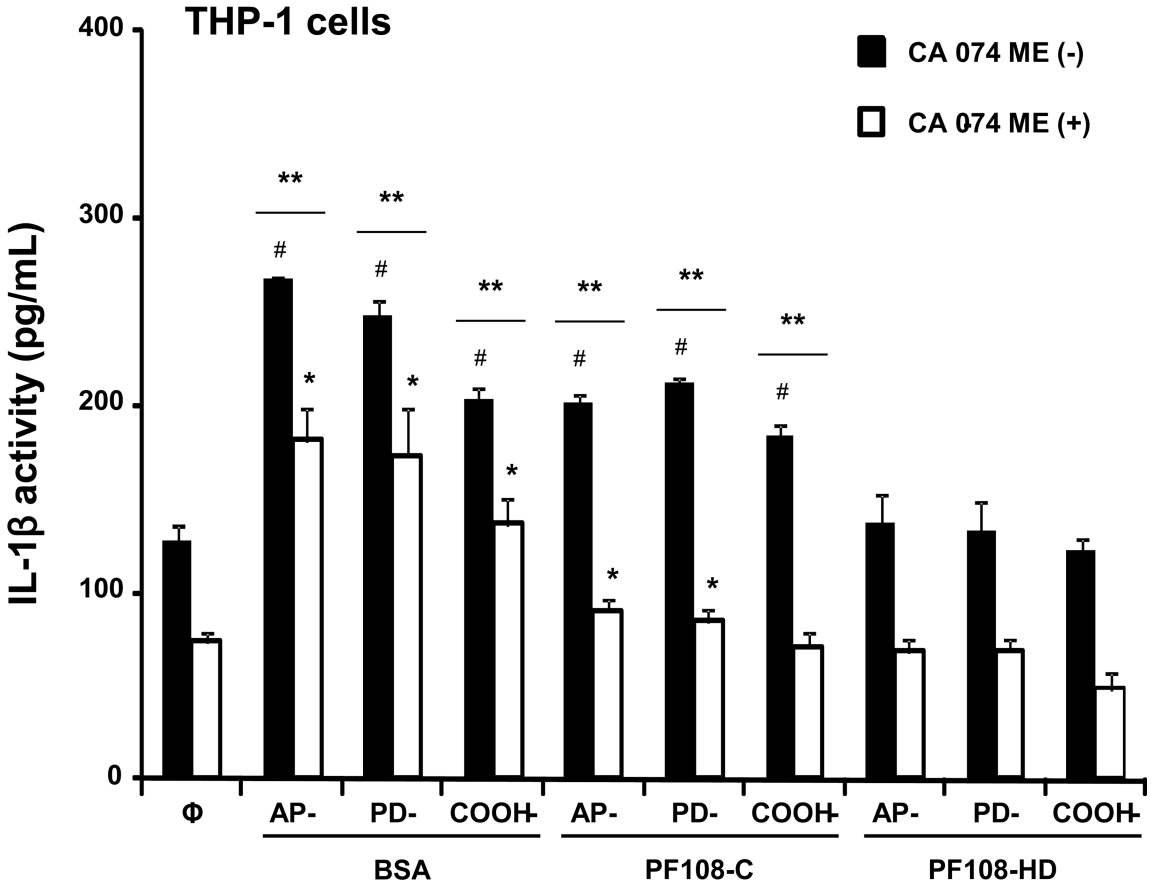

D

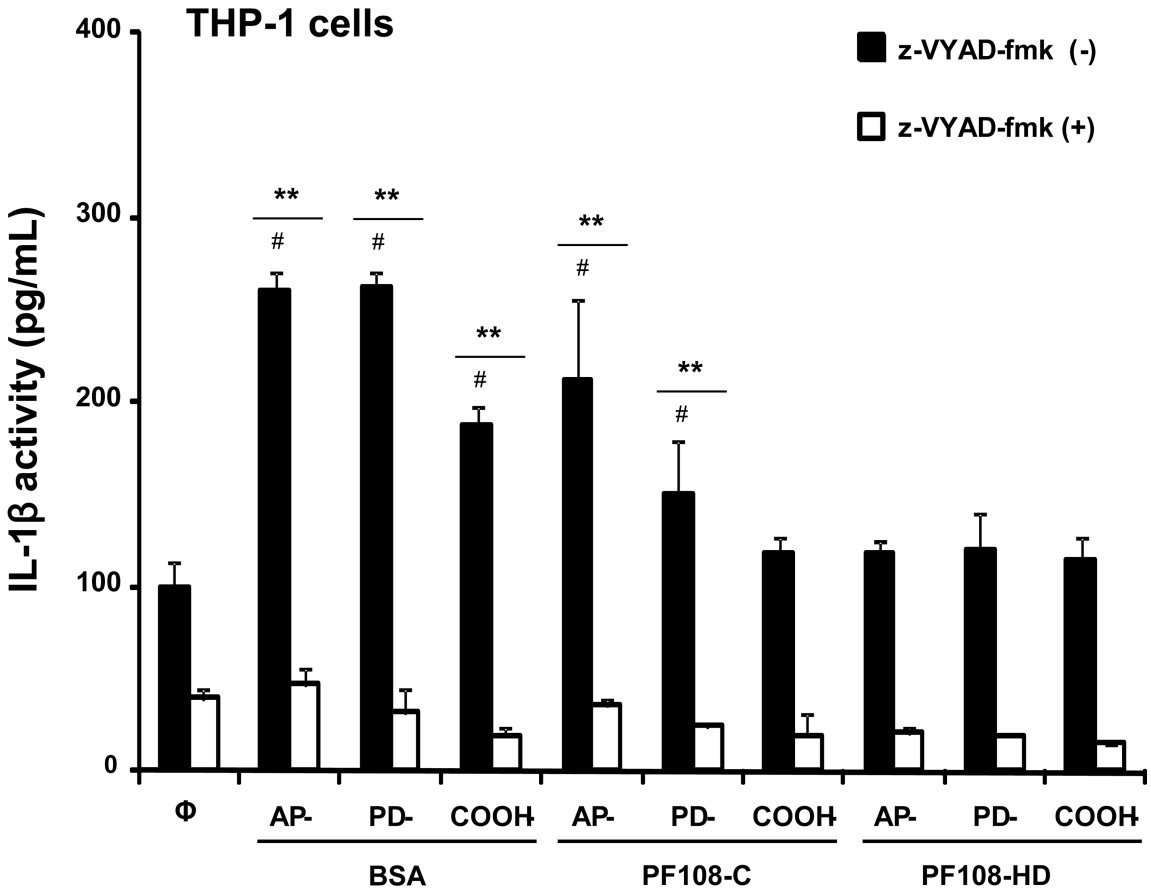

Figure 2. Comparative effect of the MWCNT dispersants on IL-1β production and NALP3 inflammasome activation in THP-1 cells

(A) THP-1 cells were treated for 24 h with the different dispersed tubes. The supernatants were collected to measure the IL-1β levels by ELISA. * denotes a p value <0.05, comparing control to CNT-exposed cells. (B) The involvement of the NALP3 inflammasome activation was confirmed by using NALP3 deficient ($NALP3^{-/-}$) and ASC deficient ($ASC^{-/-}$) HP-1 cells. None of the dispersed tubes induced IL-1β production in $NALP3^{-/-}$ and $ASC^{-/-}$ THP-1 cells. (C) The cathepsin B inhibitor, CA-074 methyl ester, and (D) the caspase 1 inhibitor, z-VYAD-fmk, were used to demonstrate the involvement of cathepsin B and caspase-1 in inflammasome activation. * $p < 0.05$, comparing control to CA-074 methyl ester or z-VYAD-fmk treated cells; # $p < 0.05$ comparing control to inhibitor free but CNT treated cells; ** $p < 0.05$ for pair-wise comparisons as shown.

A

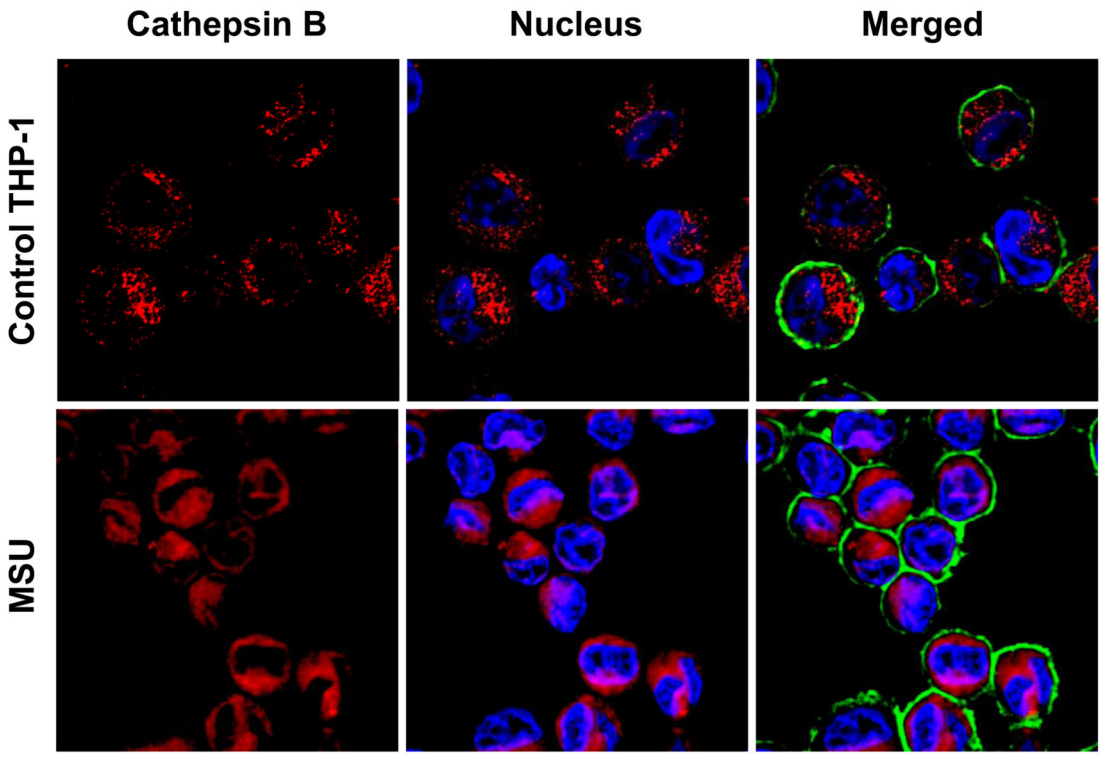

6

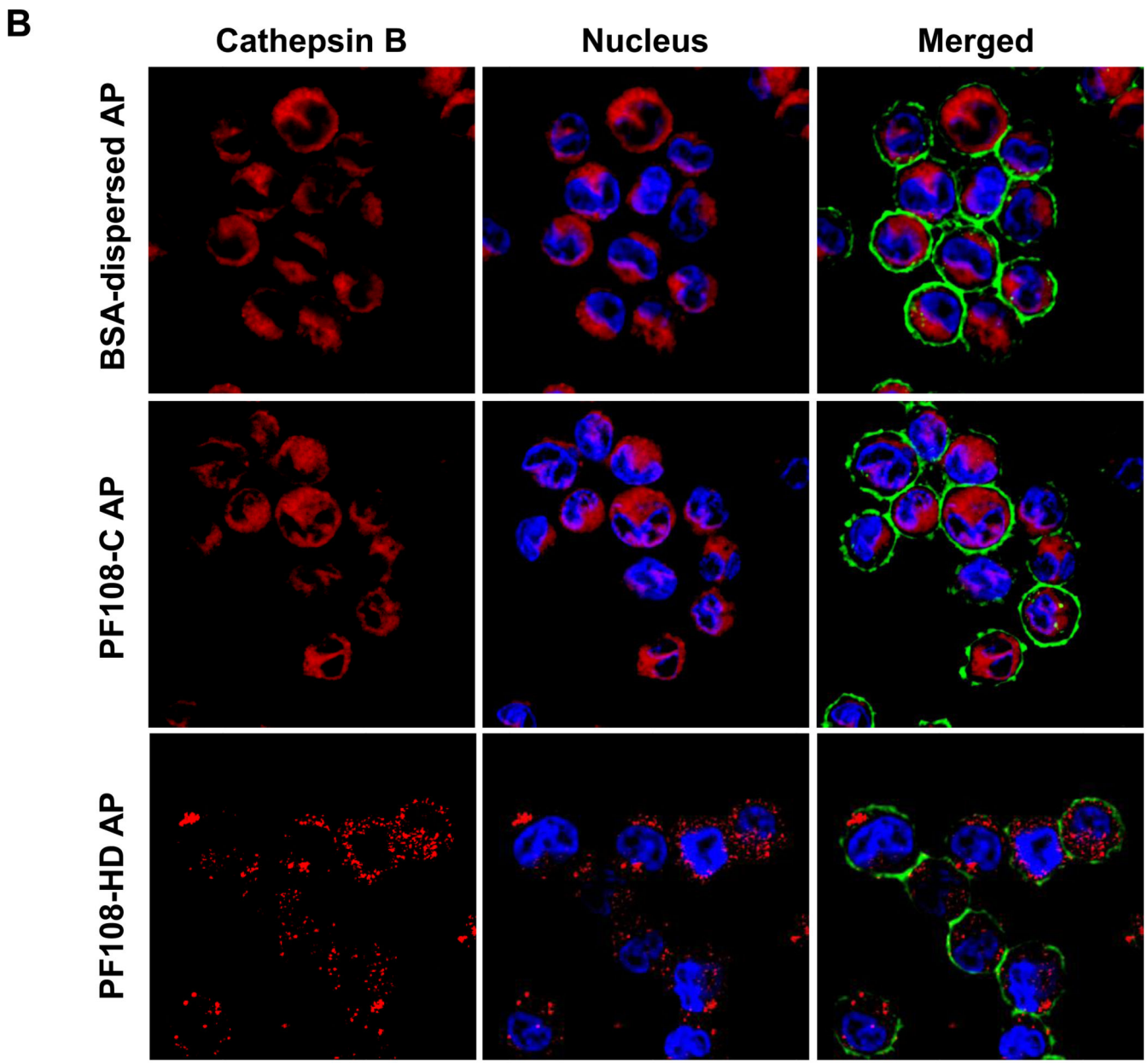

Figure 3. Confocal microscopy demonstrating the effect of different dispersants on cathepsin B release in THP-1 cells

Lysosomal damage and cathepsin B release were identified by Magic Red™ staining. THP-1 cells were seeded into 8-well chamber slides and incubated with BSA-dispersed, PF108-C and PF108-HD AP-MWCNTs at 100 μg/mL in complete RPMI 1640 for 4 h. After fixation and permeabilization, cells were stained with Magic Red™ (ImmunoChemistry Technologies), wheat germ agglutinin 633 and Hoechst 33342 dye, followed by visualization under a confocal 1P/FCS inverted microscope. (A) Use of monosodium urate (MSU) crystals as a positive control revealed that the punctate red fluorescence of Magic Red™ in the intact lysosomes of control cells changes to a diffuse red color in cytoplasm as

a result of lysosomal damage. (B) While BSA-dispersed and PF108-C tubes induced lysosomal damage, PF108-HD tubes had no effect.

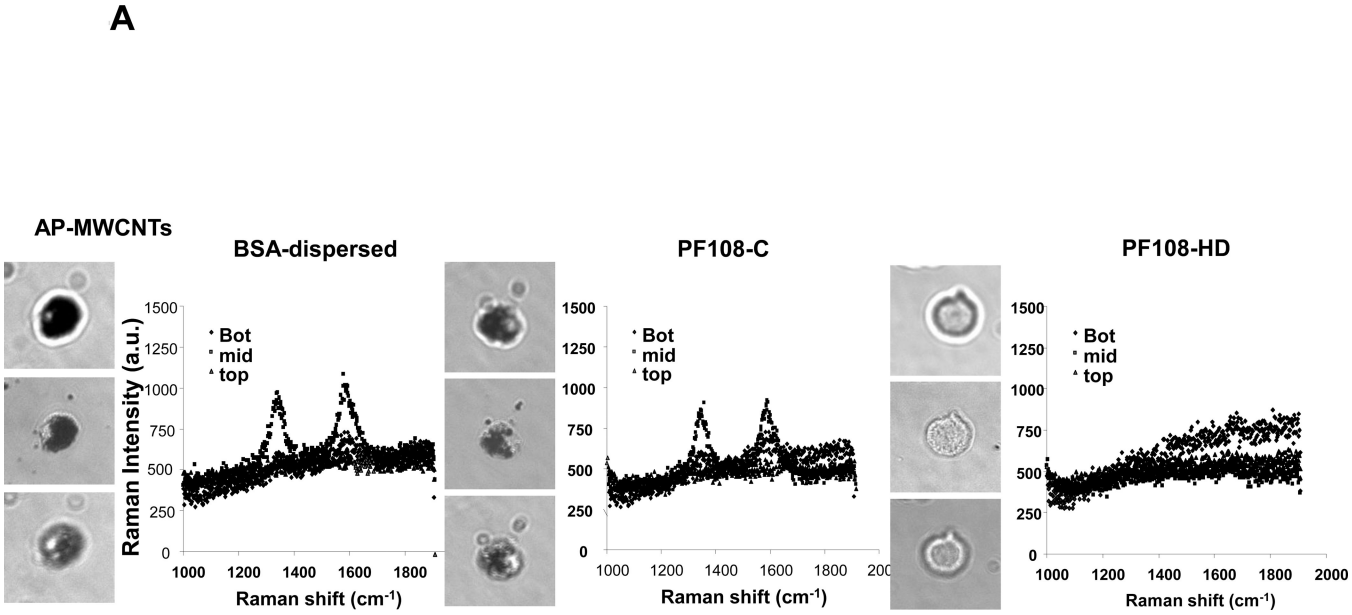

B

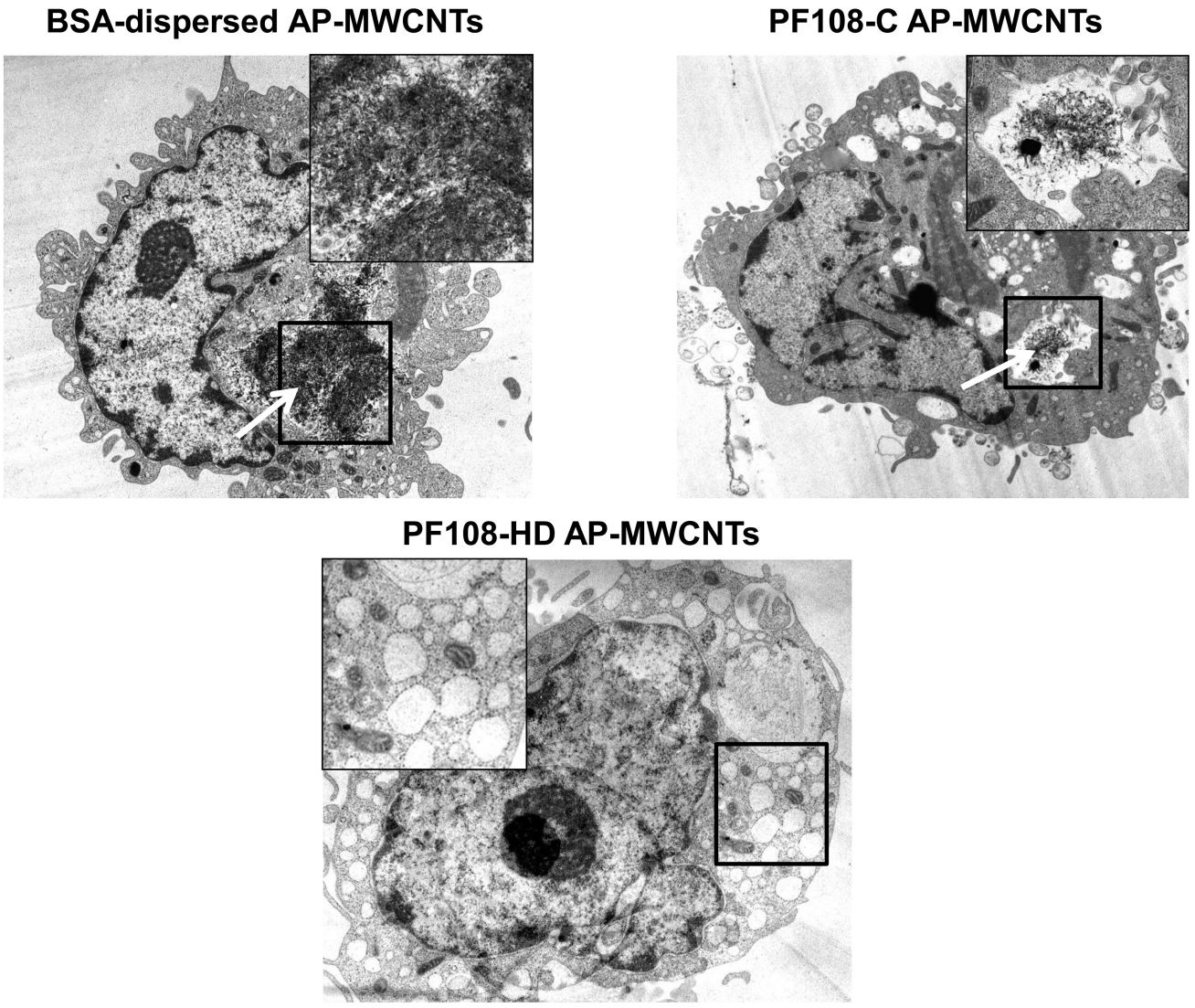

C

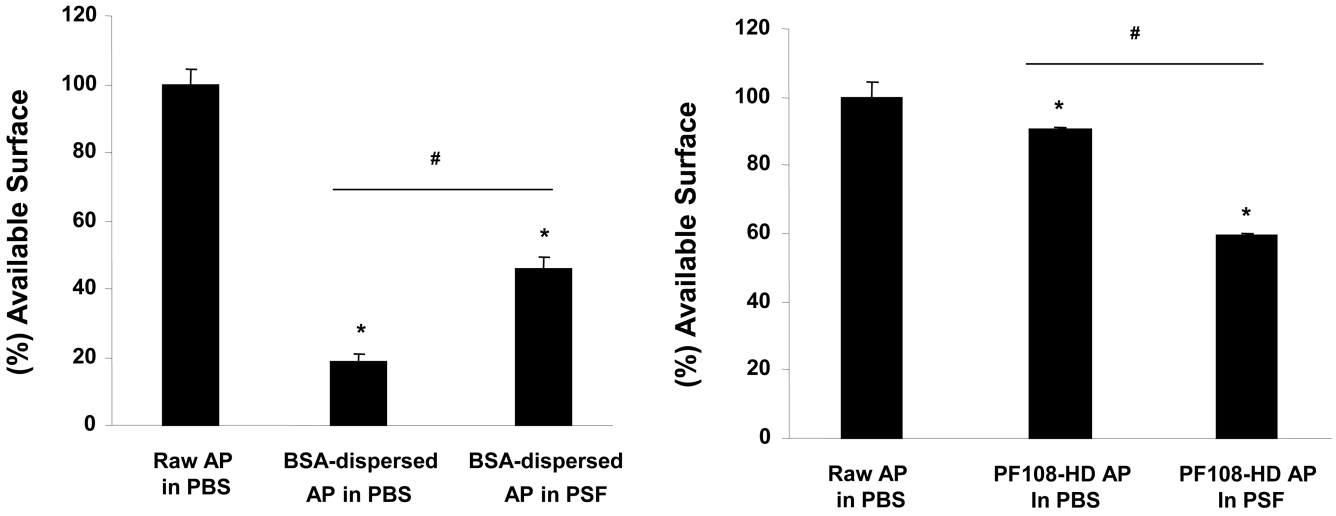

Figure 4. Assessment of the effect of the different dispersants on THP-1 uptake of AP-MWCNTs as well as FITC binding to the tubes surface

(A) Confocal Raman microscopy of THP-1 cells to show differences in the uptake of differently dispersed AP-MWCNTs. Raman spectroscopy was performed at the top, middle and bottom different cellular planes to compare signal intensities. (B) Representative TEM images to show the subcellular distribution of the dispersed tubes in THP-1 cells. The arrows point to tubes localized inside membrane-lined vesicles. Compared to BSA-dispersed and PF108-C tubes, there was little cellular uptake of PF108-HD tubes in these vesicles. (C and D) Quenching of FITC fluorescence was used to calculate the comparative surface area available for binding of this fluorophore to the surface of BSA-dispersed (C) and (D) PF108-dispersed AP-MWCNTs in PBS or PSF. The available surface of AP-MWCNTs in PBS without the addition of any dispersant was considered as 100%. The detailed calculation method is described in supplementary Materials and Methods. * $p < 0.05$ compared with available surface of AP-MWCNTs in PBS; # $p < 0.05$ for pair-wise comparisons as shown; PSF: phagolysosomal stimulant fluid.

A

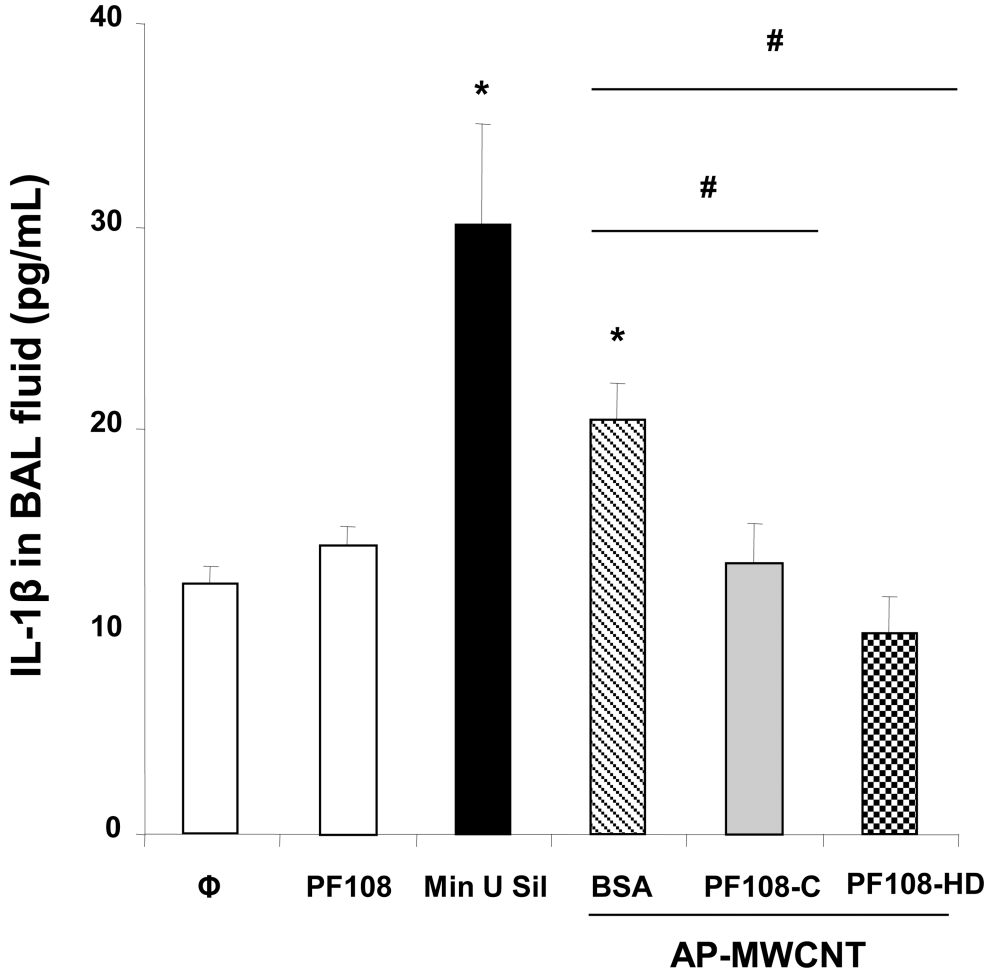

B

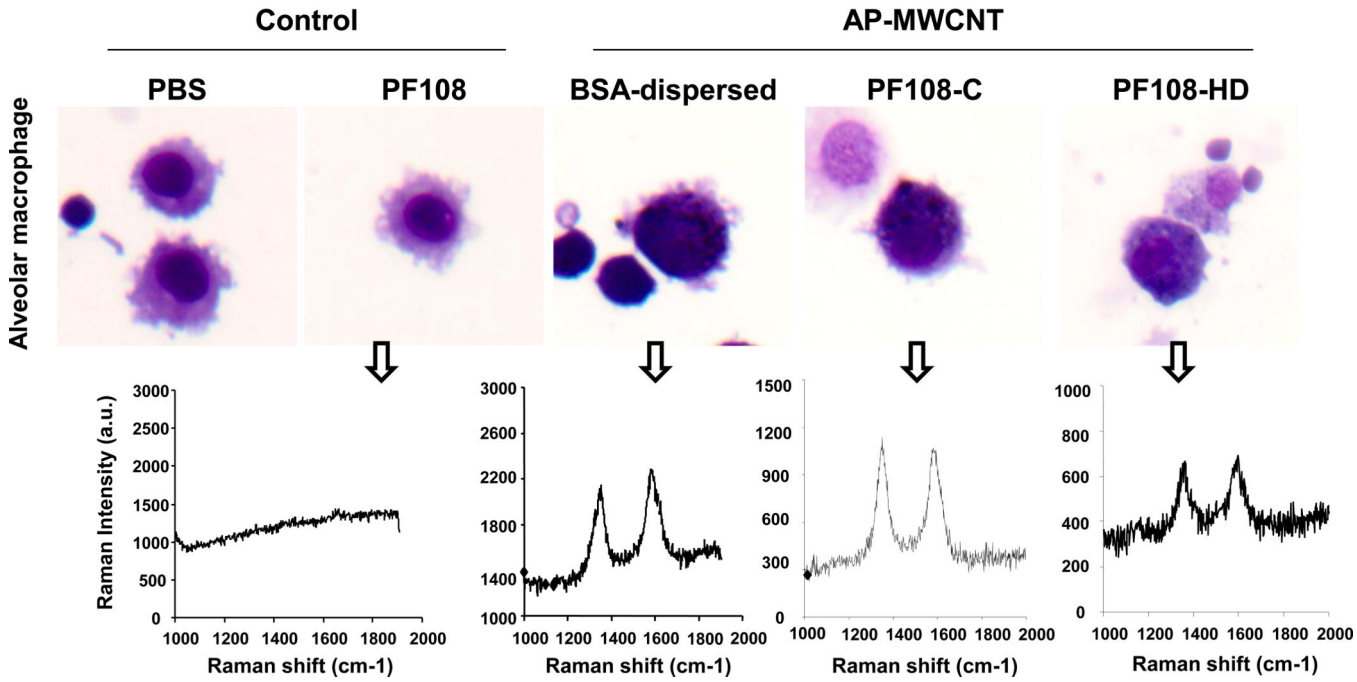

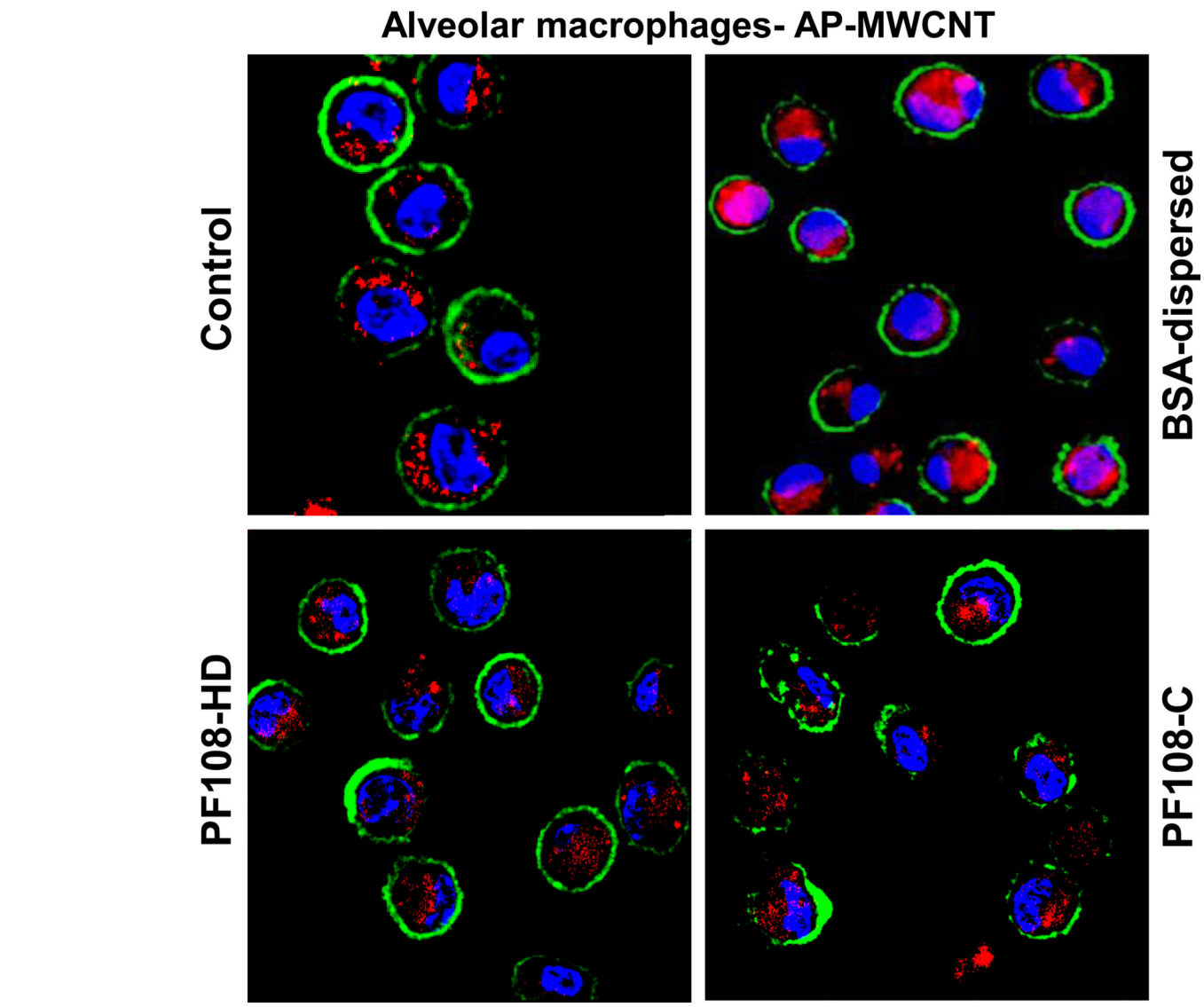

Figure 5. IL-1β production, macrophages uptake and cathepsin B release by AP-MWCNTs dispersed by BSA or PF108 in the lungs of CB57Bl/6 mice 40 h after oropharyngeal exposure

(A) C57Bl/6 mice were exposed to BSA-dispersed, PF108-C and PF108-HD AP-MWCNTs at 2 mg/kg by oropharyngeal aspiration for 40 h and BALF collected to determine IL-1β activity with an ELISA kit. 5 mg/kg Min-U-Sil served as positive control. * $p < 0.05$ compared with control; # $p < 0.05$, significant difference between BSA- and PF108-C dispersed tubes or BSA- and PF108-HD tubes. PF108-C and PF108-HD AP-MWCNTs did not induce increase of IL-1β production as opposite to significant increase by BSA-dispersed tubes. (B) The alveolar macrophages (AM) in the fluid were collected by cytospinning and staining with HEMA 2. There was no difference in AM uptake among these tubes. The intracellular presence of MWCNTs was confirmed by Raman spectroscopy, using a Renishaw inVia Raman microscope. (C) Alveolar macrophages were collected from the

BAL fluid 16 h after the mice were treated with 2 mg/kg of the different dispersed tubes. The macrophages were added to 8-well chamber slides, following which similar processing for Magic Red™ staining and performance of confocal microscopy were carried out as in Figure 3.

A

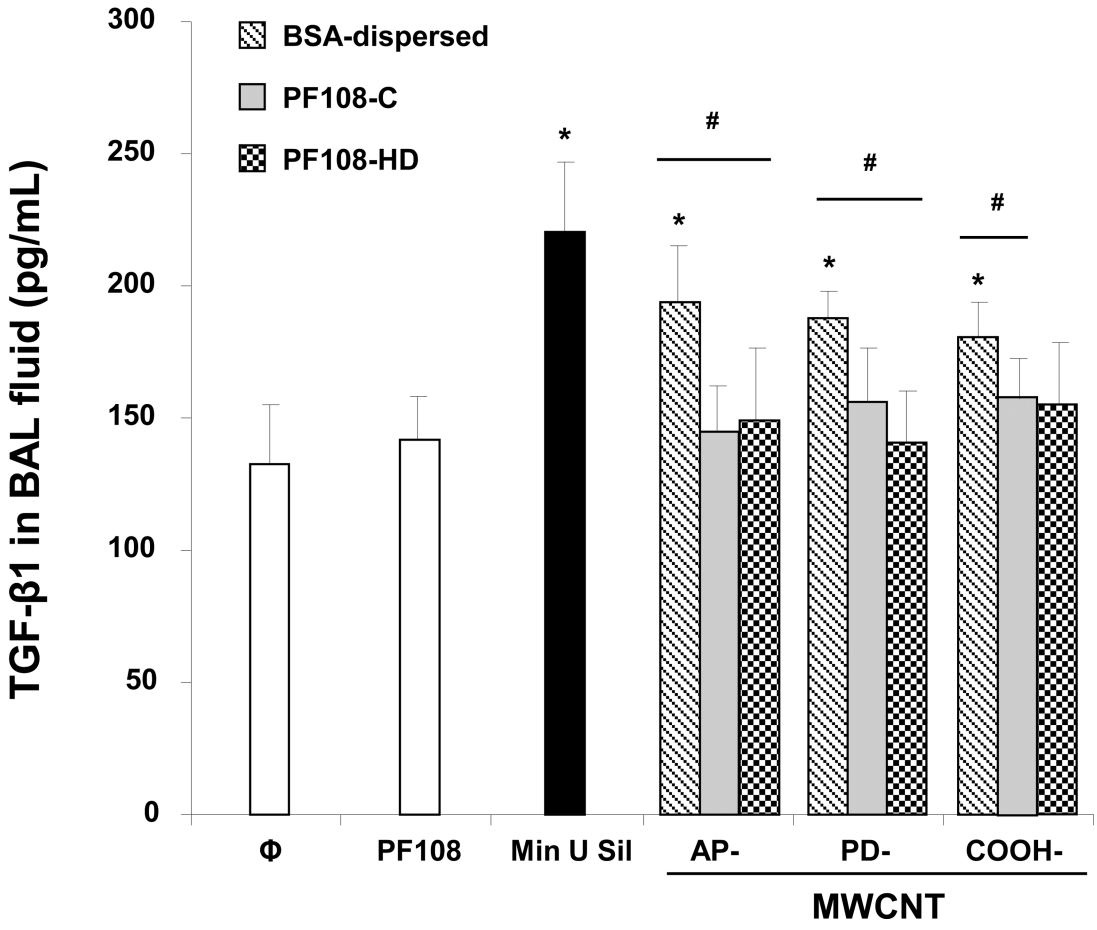

B

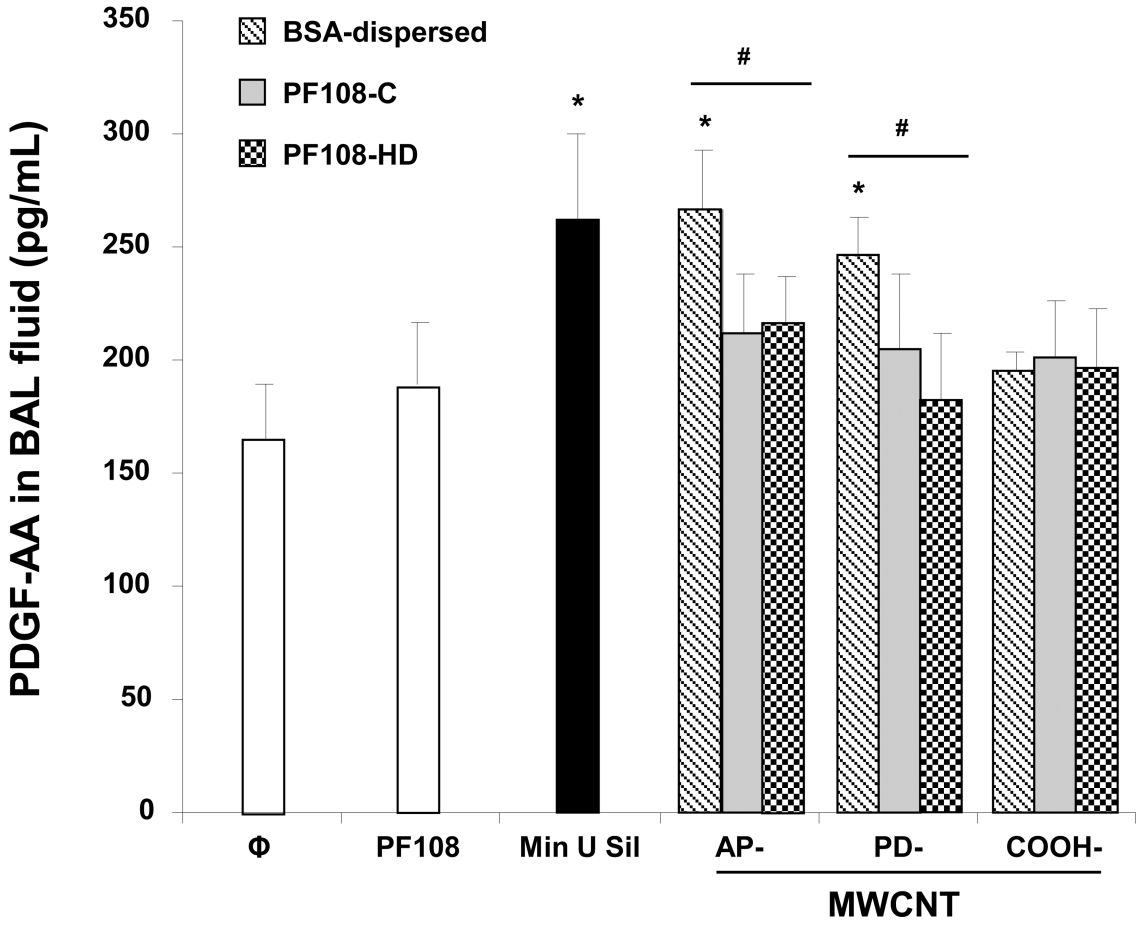

C

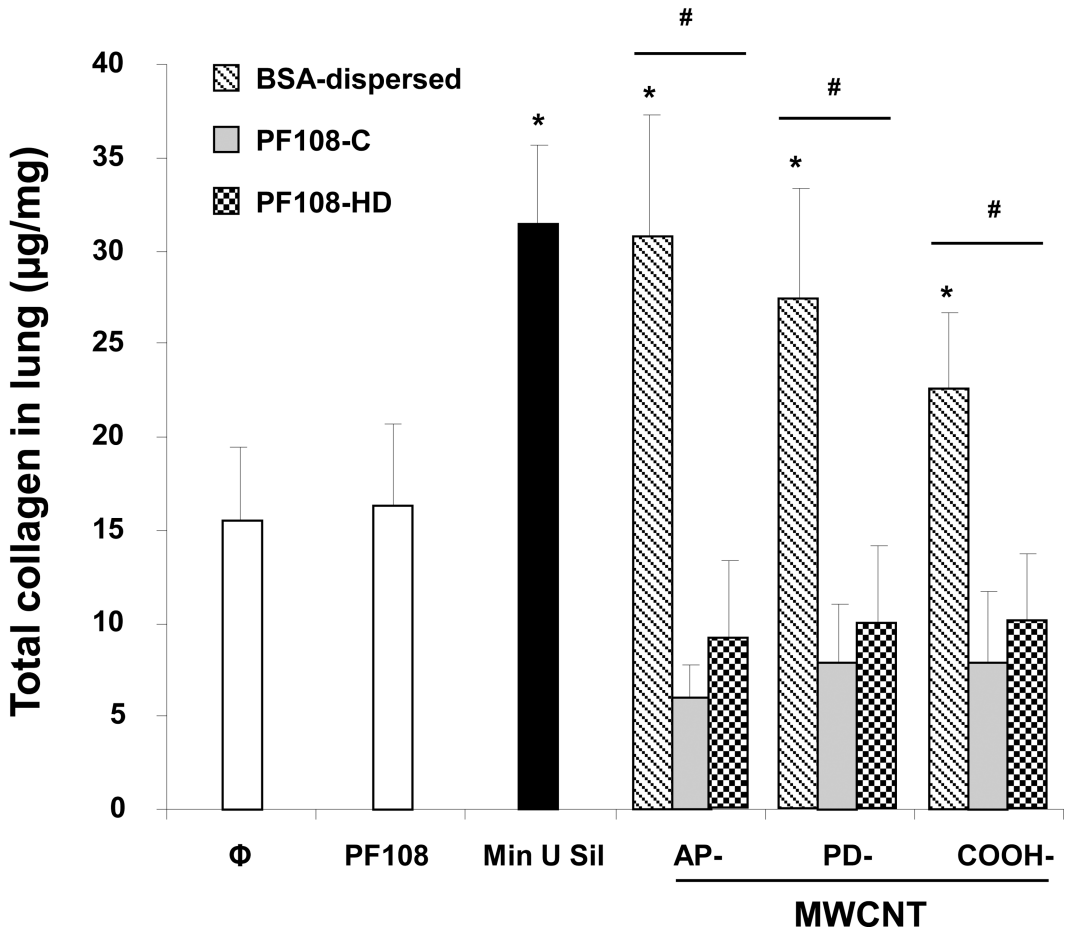

Figure 6. Comparison of the fibrotic effect of differently dispersed MWCNTs 21 days after oropharyngeal installation

The experiment described in Figure 5 was repeated, except that the mice were sacrificed 21 days after oropharyngeal inspiration of AP, PD, and COOH-MWCNTs dispersed according to the three different methods. After the animals were euthanized, fluid was collected to determine TGF-β1 (A) and PDGF-AA (B) levels. (C) Total collagen content of the lung tissue was determined using the Sircol soluble collagen assay kit (Biocolor Ltd., Carrickfergus, UK). * $p < 0.05$ compared with control, # $p < 0.05$ when comparing BSA-dispersed tubes to PF108-C and PF108-HD tubes. There were 6 animals in each group.

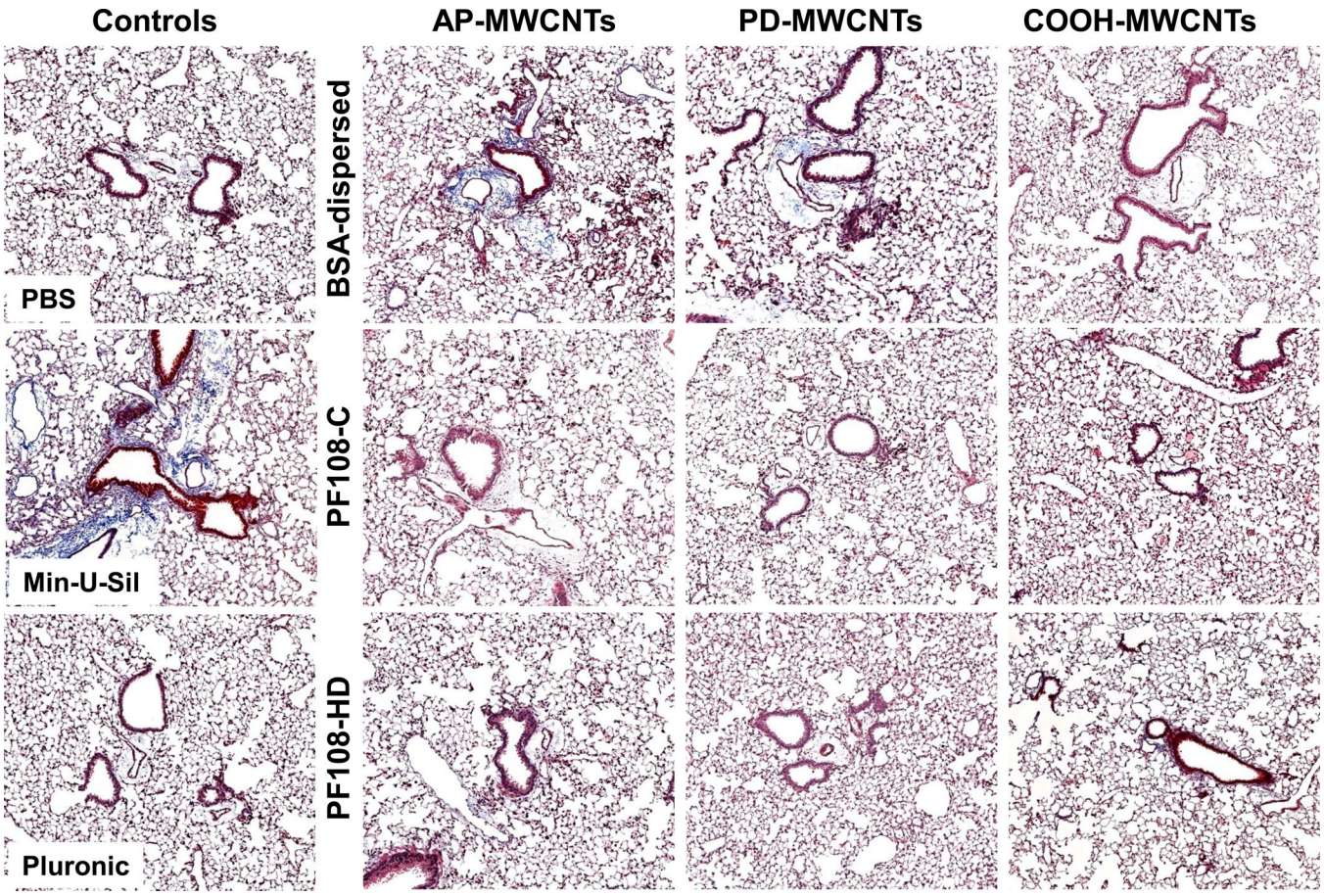

Figure 7. Collagen deposition in the lung as determined by Masson's trichrome staining

Lung tissue from the experiment described in Figure 6 was embedded, sectioned and stained with the Masson's trichrome. The blue color represents collagen staining. Lungs from Min-U-Sil exposed animals served as positive control. These lung images show at 100 × magnification are representative of the animals in each group.

Table 1

MWCNT Physicochemical Characterization

	Unit	AP-MWCNT	PD-MWCNT	COOH-MWCNT
Diameter	nm	20–30	20–30	20–30
Length in H_2O (no dispersants)	μm	5–10	5–10	5–10
Length (BSA-dispersed)	μm	1.97±0.89	2.11±0.81	1.96±0.55
Length (PF108-C)	μm	1.16±0.58	1.52±0.86	1.80±0.74
Length (PF108-HD)	μm	0.15±0.07	0.14±0.07	0.15±0.01
Size in H_2O (no dispersants)	nm	527±45	691±71	178±31
Size in H_2O (BSA-dispersed)	nm	251±58	298±41	171±43
Size in H_2O (PF108-C)	nm	151±48	197±33	163±42
Size in H_2O (PF108-HD)	nm	96±7	95±4	77±1
Surface Area	$m^2\ g^{-1}$	180	513	26
zeta potential in H_2O (no dispersants)	mV	−14.7±0.1	−10.3±1.2	−50.1±2.3
zeta potential in H_2O (BSA-dispersed)	mV	−28.6±0.8	−31.8±1.3	−29.3±1.9
zeta potential in H_2O (PF108-C)	mV	−6.9±1.1	−7.1±1.3	−10.5±1.7
zeta potential in H_2O (PF108-HD)	mV	−4.4±1.7	−5.7±0.8	−11.5±0.9
Elemental Analysis	wt.%	4.49% Ni, 0.76% Fe	1.80% Ni, 0.08% Fe	0.18% S

The average length and diameter of the tubes were assessed by TEM microscopy (JEOL 100 CX transmission electron microscope). The hydrodynamic diameters in H_2O were determined using high throughput dynamic light scattering (HT-DLS, Dynapro Plate Reader, Wyatt Technology). The zeta potential was measured using a ZetaSizer Nano-ZS (Malvern Instruments, Worcestershire WR, UK). The elemental compositions of the MWCNTs were determined by Energy Dispersive X-ray Spectroscopy (EDS, Oxford Instrument, Oxfordshire, UK). AP: as prepared; PD: purified; PF: Pluronic F108; C: crudely dispersed; HD: homogeneously dispersed.